Boundary Mixing and Topographic Blocking on the Mid-Atlantic Ridge in the South Atlantic*

A. M. THURNHERR AND K. G. SPEER

Department of Oceanography, The Florida State University, Tallahassee, Florida

(Manuscript received 4 June 2002, in final form 7 October 2002)

ABSTRACT

It is commonly observed in hydrographic sections crossing midocean ridges that the isopycnals on the ridge flanks slope downward toward the crests. Although the observed vertical scales of isopycnal dipping are not consistent with steady diffusive boundary layers on slopes, the cross-flank density gradients can nevertheless be caused by diapycnal mixing acting on timescales of several years. The corresponding pressure gradients are usually inferred to be associated with cyclonic along-flank flows. Recent observations of southward flow along the highly corrugated western flank of the Mid-Atlantic Ridge near 20°S are inconsistent with this conceptual picture, however. Data from seven zonal cross-ridge sections and from four meridional along-ridge sections were used to analyze the hydrography on the flanks of the Mid-Atlantic Ridge between 2°N and 30°S. The majority of the hydrographic stations were occupied over deep cross-flank canyons, which extend over a total length of ~90 000 km in the tropical and subtropical South Atlantic alone. The dipping of the isopycnal surfaces on the western ridge flank in the Brazil Basin is largely restricted to the canyons, where flow along the flank is topographically blocked. The magnitudes of the blocked apparent along-ridge transports are typically of order 1 Sv (1 Sv $\equiv 10^6$ m^3 s^{-1}) with values as high as 3 Sv, implying important consequences for circulation studies with both forward and inverse models. In the southern Brazil Basin the horizontal density gradients immediately above the blocking topography are reversed—that is, the densities increase toward the crest of the Mid-Atlantic Ridge, consistent with observations of southward flow along the flank. On the eastern flank in the Angola Basin there is a layer of crestward-increasing densities as well, but there it lies well above the ridge topography. Numerical solutions of the buoyancy equation indicate that the observed cross-flank density gradients of both signs are consistent with bottom-intensified diapycnal mixing, which causes a vertical buoyancy-flux dipole. Boundary mixing on slopes can therefore give rise to anticyclonic, as well as cyclonic, along-slope flows. The observed horizontal temperature and salinity gradients near the Mid-Atlantic Ridge in the South Atlantic cannot be accounted for by diapycnal mixing alone, on the other hand. The distributions of these properties are therefore largely determined by isopycnal processes.

1. Introduction

It is commonly observed in hydrographic sections crossing midocean ridges that the isopycnals (and isotherms) on ridge flanks slope downward toward the crests (e.g., section 3). This effect is sometimes interpreted as a boundary layer signature, primarily because of its qualitative similarity with diffusive boundary layers of stratified fluids on slopes (Wunsch 1970; Phillips 1970). In a steady state without flow in the linearly stratified interior (constant buoyancy frequency N), and with constant mixing coefficients for momentum (ν) and heat (κ), the boundary layer thickness (e-folding scale) on a planar slope in a rotating system is given by (e.g., Garrett et al. 1993)

$$\delta = \left(\frac{f^2}{4\nu^2} + \frac{N^2 \sin^2\alpha}{4\nu\kappa} \right)^{-1/4}, \qquad (1)$$

where f and α are the Coriolis parameter and the slope angle, respectively. When representative values for the midocean ridge slope ($\alpha = 2 \times 10^{-3}$) and for the deep-ocean stratification ($N = 10^{-3}$ s^{-1}) are chosen, and when a Prandtl number of order unity is assumed (i.e., $\nu \approx \kappa$) the first summand dominates, except within ≈1° of the equator, and the bottom boundary layer is essentially in Ekman balance. In order for an Ekman layer at 10° latitude to extend over a thickness (two e-folding scales) of 1000 m, consistent with observations (e.g., Thompson and Johnson 1996), an improbably large eddy viscosity of $\nu \approx 3$ m^2 s^{-1} is required. [The thickness of the nonrotating boundary layer is given by expression (1) with vanishing f (Wunsch 1970; Phillips 1970) and requires mixing coefficients $>10^{-1}$ m^2 s^{-1} to account for the observations.] The observed dipping of isopycnals on ridge flanks is therefore not consistent with

Corresponding author address: A. M. Thurnherr, Department of Oceanography, The Florida State University, Tallahassee, FL 32306-4320.
E-mail: a.thurnherr@ocean.fsu.edu

steady-state diffusive boundary layer scales. Thompson and Johnson (1996) show that the hydrographic observations on some midocean ridge flanks are nevertheless consistent with bottom-enhanced diapycnal mixing. The reason for this is that a steady-state diffusive boundary layer on a rotating slope implies a particular along-slope flow in the interior and the adjustment toward this flow takes place diffusively (e.g., Garrett et al. 1993). In the cases investigated by Thompson and Johnson (1996) the timescales of adjustment $\tau = \delta^2/(4\kappa)$ are of the order of decades.

Away from the equator the cross-slope pressure gradients associated with the dipping isopycnals are usually presumed to be balanced by geostrophic velocity shear. The implied along-slope flows are equatorward on the western flanks and poleward on the eastern flanks of meridional midocean ridges in both Northern and Southern Hemispheres (e.g., Thompson and Johnson 1996; Huang and Jin 2002). However, the available observational evidence for flank flows in the South Atlantic is inconsistent with such a cyclonic tendency. Float displacements and trajectories at 4000 m (Hogg and Owens 1999), tracer-advection observations (Ledwell et al. 2000a), and inverted hydrographic and microstructure data (St. Laurent et al. 2001) all indicate poleward velocities of approximately 2×10^{-3} m s^{-1} on the western flank of the Mid-Atlantic Ridge (MAR) near 20°S. Above the eastern flank Warren and Speer (1991) infer equatorward flow at 11° and 24°S. The observed current directions on both flanks are therefore opposite to those expected from the dipping isopycnals.

In the data analyzed by St. Laurent et al. (2001) the dipping of the isopycnal surfaces on the western flank of the MAR near 20°S is confined within ridge-flank canyons, where topographic blocking prevents the cross-flank pressure gradients from being balanced geostrophically by along-flank flow. An advective–diffusive heat budget of such a canyon indicates that a steady state requires mean crestward along-canyon flow down the pressure gradient. The presence of canyons or valleys therefore creates circumstances important for the circulations associated with diapycnal mixing on slopes. Mean downgradient flows in deep submarine valleys can themselves give rise to processes that are associated with strong mixing, such as hydraulically controlled cross-sill flows and topographic lee waves (Thurnherr and Richards 2001; Thurnherr et al. 2002). This implies that it may be the presence of the ridge-flank canyons on the western flank of the MAR in the South Atlantic, and not just processes associated with random topographic variance or roughness (Polzin et al. 1997; Jayne and St. Laurent 2001), that is responsible for the high rates of mixing observed there. [Tidal modulation of the observed dissipation levels (Ledwell et al. 2000b) does not necessarily imply that the mixing energy is derived from the tides. Other processes that are associated with strong mixing, such as hydraulic exchange flows, can also be tidally modulated (e.g., Helfrich 1995).]

In order to close the global overturning circulation, the production of dense water at high latitudes must be balanced elsewhere by upward vertical motion and downward diffusion of buoyancy (e.g., Munk 1966). While it is not currently feasible to observe the vertical motion directly, the spatial distribution of diffusivity can be inferred from velocity- and temperature-microstructure data (e.g., Gregg 1998) validated by tracer-release experiments (e.g., Ledwell et al. 2000b). Observations in the Brazil Basin indicate that much of the diapycnal mixing there takes place on the flank of the MAR (Polzin et al. 1997), and Morris et al. (2001) conclude that the buoyancy budget for the bottom water can be closed by mixing on the ridge flank. Jayne and St. Laurent (2001) provide evidence for the global importance of ridge-flank mixing by showing that parameterizing dissipation as a function of seafloor roughness improves the surface-elevation signature of a global barotropic tidal model. With their parameterizations the rates of tidal dissipation (and, presumably, the diapycnal fluxes) are greatly increased throughout large areas of the deep ocean.

The main purpose of this study is to present an analysis and dynamical interpretation of hydrographic data from the flanks of the MAR between 2°N and 30°S. First we show that the roughness of the ridge over much of the domain is highly organized as a sequence of deep cross-flank canyons (section 2). These are so common, in fact, that a large percentage of the available hydrographic stations in both meridional and zonal sections extend significantly below the crest depths of the lateral canyon walls, where along-flank flows are topographically blocked. In section 3 we show that on the western flank in particular the dipping of isopycnal surfaces observed in zonal sections takes place primarily within the ridge-flank canyons. Calculating geostrophic flows from the zonal density gradients without taking topographic blocking into account results in unrealistic apparent along-flank transports with magnitudes of order 1 Sv (1 Sv $\equiv 10^6$ m^3 s^{-1}). The cross-flank hydrographic gradients rise significantly above the interannual variability, allowing their meridional distributions to be inferred from nonsynoptic hydrographic data (section 4). The results show that isopycnal dipping takes place along the entire length of both ridge flanks in the South Atlantic and that on the western flank it is largely confined within the canyons. There are regions above both ridge flanks where the densities increase toward the crest. In particular, the density field in the Brazil Basin near 20°S is consistent with direct observations of poleward flow along the ridge flank. Numerical solutions of the density, heat and salt equations indicate that the observed cross-flank density gradients on the MAR are consistent with bottom-intensified vertical mixing acting on time scales of the order of years, while the horizontal distributions of temperature and salinity are primarily determined by isopycnal processes (section 5). The main results are discussed in section 6.

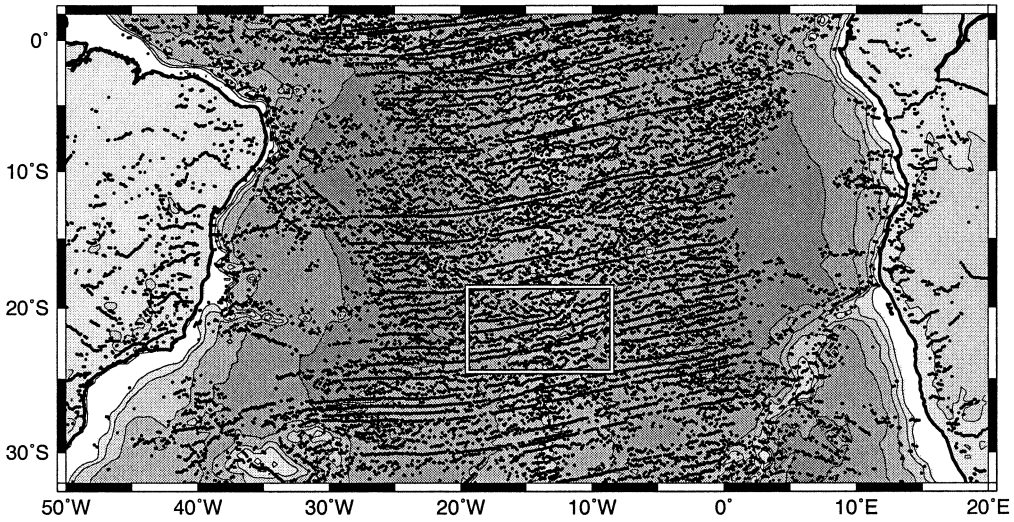

FIG. 1. Local depth maxima (dots) in meridional sections of the South Atlantic seafloor topography. Bathymetric contours are derived from 9 × 9 pixel block-averaged data of Smith and Sandwell (1997, version 8.2); contour interval is 1000 m. Depth maxima are taken from full-resolution meridional sections, separated by 5′ of lon, and subsampled every 5 km; successive maxima at a given lon are separated by depth minima at least 250 m shallower. The frame indicates the extent of the region shown in Fig. 3.

2. Ridge-flank topography and hydrographic stations

In the inversion of St. Laurent et al. (2001) the topographic organization of the western flank of the MAR near 20°S is crucial: it is only in the deep cross-flank canyons that a priori constraints of negative diapycnal advection, implied by monotonically increasing dissipation toward the seabed and the choice of a constant mixing efficiency, is overcome by other constraints allowing water to gain buoyancy along the path of the flow. A steady-state density field is maintained by diapycnal mixing balancing horizontal advection of buoyancy. In another deep submarine valley with similar topographic and hydrographic characteristics there are direct observations of mean along-valley downgradient flow on timescales of months to years (Keller et al. 1975; Thurnherr and Richards 2001; Thurnherr et al. 2002), implying a similar balance.

Meridional topographic sections along both flanks of the MAR are characterized by approximately regularly spaced bathymetric minima and maxima, consistent with high-resolution maps of the seafloor topography showing a large number of canyons cutting across the ridge flanks. These canyons can be visualized by plotting the locations of local depth maxima in closely spaced meridional topographic sections (Fig. 1). The horizontal resolution of the Smith and Sandwell (1997) seafloor topography ($\leq 1/30°$) is sufficient for tracing the ridge-flank canyons, which are meridionally separated by $\approx$60 km. Because we are ultimately interested in blocking of along-flank flows (section 3), only depth maxima meridionally separated by minima at least 250 m shallower are shown. [In order for a 2D topographic obstacle to effectively block uniform nonrotating flow $Nh/U \gtrapprox 2$, where h and U are the obstacle height and the flow velocity, respectively (e.g., Baines 1987). Rotating flows are blocked by 2D Gaussian obstacles of even lesser height (Pierrehumbert and Wyman 1985). Using conservative values for $N = 5 \times 10^{-4}$ s^{-1} and for $U = 5 \times 10^{-2}$ m s^{-1}, the limiting criterion becomes $h \geq 200$ m.] Figure 1 confirms that much of the ''roughness'' on both ridge flanks, which covers more than 50% of the seafloor in our study region, is organized as a sequence of cross-flank canyons. Inspection of individual meridional sections indicates that the canyon depths range between a few hundred and a thousand meters. The distribution of depth maxima in zonal topographic sections appears much more random than Fig. 1. Only a few quasi-meridional valleys, such as the rift-valley segments on the crest of the MAR, stand out visually. A simple valley-detection algorithm (see the appendix) confirms that the ridge-flank canyons are primarily zonal and that the topographic characteristics of both flanks are similar (Table 1).

TABLE 1. Total lengths of connected valley segments longer than 40 km below 1500 m in the South Atlantic between 2°N and 30°S; see the appendix for details of valley-detection algorithm.

	Western basin	Eastern basins	Total
Zonal valleys	47 000 km	40 000 km	87 000 km
Meridional valleys	9000 km	6000 km	15 000 km

Figure 2 shows the hydrographic stations used in this study. The western and eastern abyssal basins are the Brazil Basin and the Angola Basin, respectively. The

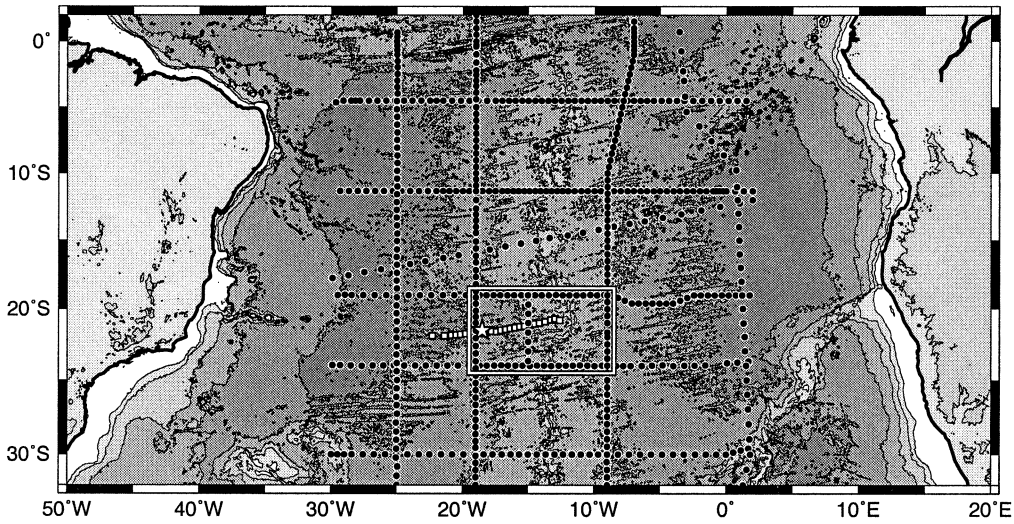

FIG. 2. Hydrographic stations on the MAR in the tropical and subtropical South Atlantic. Bathymetric contour interval (full-resolution data; cf. Fig. 1) is 1000 m; bullets show CTD stations; the star indicates the location of a 6× HRP repeat station; open squares mark the canyon analyzed by St. Laurent et al. (2001); the frame indicates the extent of the region shown in Fig. 3.

dataset, which covers the MAR (30°W–2°E; Fig. 1), is a combination of conductivity–temperature–depth (CTD) profiles from the pertinent World Ocean Circulation Experiment (WOCE) hydrographic sections (A07–A10, A14, A15), as well as from a number of high-quality pre-WOCE sections: Ajax 1 (e.g., Stramma and Peterson 1990), Oceanus 133 (e.g., Warren and Speer 1991), and SAVE 2 and 6 (e.g., DeMadron and Weatherly 1994). The salinity measurements are adjusted for mutual consistency at section crossovers using a method similar to the one described by Johnson et al. (2001) (see online at http://www.ocean.fsu.edu/SAC). In order to assess the temporal variability of the hydrography we also use observations from a high-resolution profiler (HRP) 6× repeat station of the dataset described by Polzin et al. (1997), as well as two stations from the survey analyzed by St. Laurent et al. (2001). The HRP temperature and pressure sensors were calibrated before and after each cruise and the salinities were adjusted by fitting the deep temperature–salinity (T–S) properties to profiles from nearby CTD stations occupied during the same cruises (J. M. Toole 2002, personal communication).

The typical meridional distance between neighboring ridge-flank canyons is similar to the station spacing of the WOCE sections. Figure 3 shows hydrographic stations in the context of the seafloor topography in a subregion of the MAR. A significant portion of the stations was occupied over canyons, especially in the meridional sections at 19° and 15°W on the western ridge flank. In the case of the zonal sections at 19° and 24°S the situation is somewhat less clear but the 24°S section most closely follows what might be considered a continuous valley between 17° and 14°W.

Figure 4 illustrates the topographic context of the hydrographic stations at 19°W shown in Fig. 3. Several CTD profiles extend below the Smith and Sandwell (1997) seafloor—in one case (station 94), by more than 600 m. Both navigational uncertainties and depth errors in the bathymetric data are possible causes. The ridge-flank canyons are typically ≈500 m deep. In conjunction with the characteristic ridge-flank slope of $\alpha \approx 2 \times 10^{-3}$ this implies cross-flank excursions of the isobaths of several hundred kilometers, consistent with the bathymetric contours shown in Figs. 2 and 3.

Most of the CTD profiles collected on the MAR extend into the ridge-flank canyons where along-flank flows are topographically blocked. In order to estimate the depths below which this blocking occurs the meridional extent of the topographic influence is required. It seems reasonable to assume that a geostrophic along-flank flow of width l does not follow the isobaths into a cross-flank canyon narrower than l. On steep slopes (relative to f/N) the cross-slope width of a geostrophic along-slope flow scales with the Rossby radius of deformation Nh/f, where h is the vertical scale of the current. This is the appropriate regime for canyons cutting across typical continental shelves, where slow along-slope flows follow the isobaths into and out of canyons that are wide compared to the local Rossby radii (e.g., Klinck 1996). The horizontal-to-vertical aspect ratios of flows along shallow slopes, on the other hand, are determined by the slope angles (e.g., Stommel and Arons 1972)—that is, $l = h/\tan\alpha$. Using a conservative value for the stratification on the western flank of the MAR ($N = 10^{-3}$ s^{-1}; Fig. 4) to assess the steepness of the ridge flank yields $\tan\alpha < f/N$, except within ≈1° of the equator. Together with the vertical scale of the coherent cross-slope density gradients on the ridge flanks ($h = 500$ m; section 4) this implies a minimum

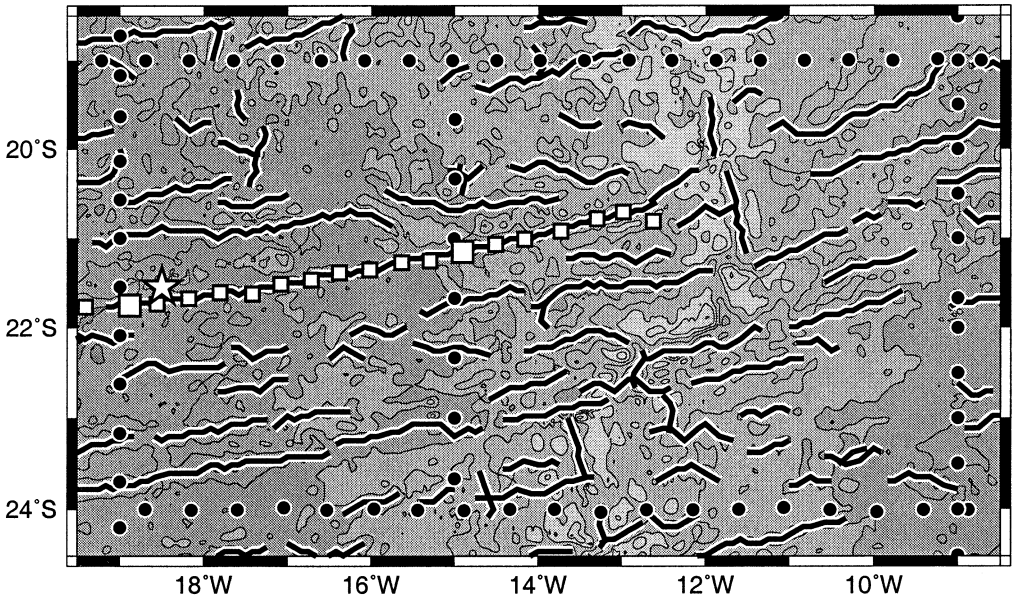

FIG. 3. Hydrographic stations (symbols) and valley segments (lines) in a relatively densely sampled region of the MAR (framed in Figs. 1 and 2). Bathymetric contour interval is 500 m; bullets show CTD stations; the star indicates the location of a 6× HRP repeat station; open squares mark the canyon analyzed by St. Laurent et al. (2001), with the larger symbols indicating the HRP station positions used to calculate a synoptic cross-flank density-difference profile at 22°S (Fig. 7); heavy lines show automatically detected zonal and meridional valley segments longer than 40 km (see the appendix for details).

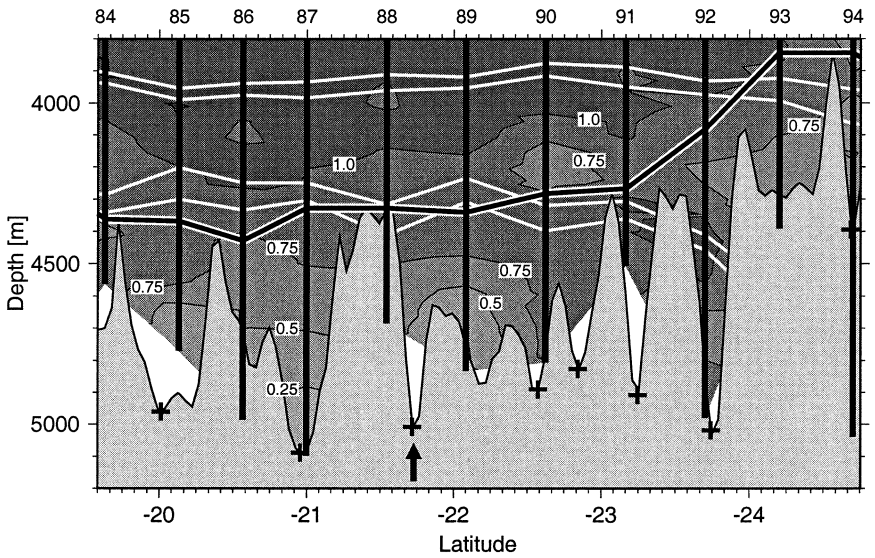

FIG. 4. Buoyancy frequencies (shaded) and neutral-density surfaces (unlabeled white contours) at 19°W. Buoyancy frequencies are calculated in 150-m-thick layers; contours are labeled in units of 10^{-3} s^{-1}; extrapolated values in the bottom triangles are not shown. The neutral-density surfaces at 28.16($\pm$0.003) and 28.20($\pm$0.003) correspond to layer interfaces in the inversion of St. Laurent et al. (2001); 0.003 is the approximate isobaric high-frequency standard deviation of density (section 3). Crosses on the seafloor indicate the locations of local depth maxima (cf. Fig. 1). The black-on-white topography-following line illustrates the blocking depth for along-flank flow. The vertical lines show CTD profiles of the WOCE A09 section; station numbers are indicated above the panel. The arrow near 21°45′S marks the canyon analyzed by St. Laurent et al. (2001).

width of 250 km for the cross-flank canyons into which along-flank flows are expected to follow the isobaths. Because there are regions where the slope of the MAR is perhaps twice the mean value the topographic blocking depth for along-flank flows is conservatively set to the minimum depth in 1°-wide meridional windows centered at the latitudes of the CTD stations. This is illustrated by the black-on-white line following the topographic peaks in Fig. 4. In the case of zonal sections the blocking depth for the geostrophic flow between a given station pair is set to the average blocking depth between the stations.

The neutral-density surfaces shown in Fig. 4 are qualitatively consistent with this choice of blocking depth. The 4000-m float displacements and trajectories of Hogg and Owens (1999), the tracer-advection observations of Ledwell et al. (2000a), and the inversion of St. Laurent et al. (2001) all indicate southward along-flank flow at 19°W in the layer between the 28.16 and 28.20 neutral surfaces in this latitude band. [At densities greater than 28.20 the along-flank flow diagnosed by St. Laurent et al. (2001) is restricted to the region west of 19°W, i.e., further down in the Brazil Basin.] If the along-flank current were following the isobaths below the blocking depth we would expect the isopycnals to drop between the walls of wide valleys, especially between stations 88 and 91 (180-km distance; see also Fig. 3).

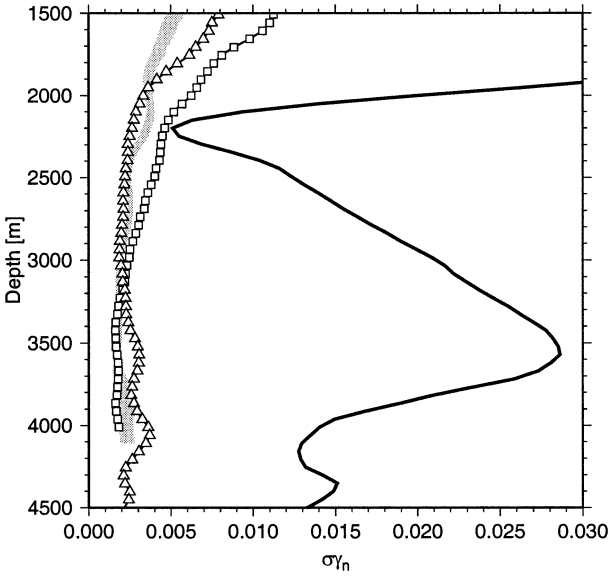

FIG. 5. Isobaric neutral-density variability estimated from repeat stations. Gray band: min–max range in 50-dbar bins of std dev calculated at 2-dbar intervals from western-flank HRP data at a station occupied 6× in 2 weeks in 1996 (stars in Figs. 2 and 3). Profiles plotted with symbols: meridionally averaged standard deviations in 50-dbar bins calculated from repeat stations at section crossovers on the ridge flanks at 19°W (triangles) and at 9°W (squares). Solid line: standard deviations in 50-dbar bins calculated from a repeat station at 18.7°S/19°W occupied twice (station numbers 82 and 112) in 11 days during WOCE A15 in 1994. All profiles are smoothed with a 150-m running boxcar.

3. Topographic blocking of along-flank flows

In order to analyze the ridge-flank hydrography in detail it is useful to investigate its temporal variability. The high-frequency neutral-density variance at a given location on timescales of hours to weeks (primarily related to internal waves and tides) is estimated from a western-flank HRP repeat station that was occupied six times during two weeks in 1996 (stars in Figs. 2 and 3). The resulting standard deviations (gray band in Fig. 5) indicate a typical variability of $\approx 3 \times 10^{-3}$ neutral-density units below the crest depth of the MAR ($\approx$2500 m). This corresponds to vertical displacements of the isopycnal surfaces of order 50 m. (All density-related terms in this study refer to neutral density, the units of which will be omitted below.) The density variability on longer timescales is estimated from crossovers of hydrographic sections at 19° and 9°W on the ridge flanks (Fig. 2). The resulting profiles, plotted with symbols in Fig. 5, indicate that the standard deviations of neutral density over the total sampling period (12 yr) below crest depth are $\leq 5 \times 10^{-3}$ on both flanks. Anomalous properties in eddies can give rise to hydrographic observations significantly outside the expected variability, however. During the WOCE A15 cruise, for example, a station at 18.7°S, 19.0°W was occupied twice in 11 days. The solid line in Fig. 5 shows the neutral-density standard deviations (i.e., half the isobaric density differences) estimated from this repeat station. Below 4100 m, where the density differences correspond to vertical displacements of the isopycnal surfaces of up to 400 m, the *T*–*S* properties of the two profiles agree closely, indicating that the variability is real and not caused by measurement errors. [Weatherly et al. (2002) have recently carried out a detailed analysis of these and other hydrographic and tracer signatures associated with abyssal eddies in the Brazil Basin.]

The quantitative estimates of the temporal variability facilitate interpretation of the hydrographic data. The top panels in Fig. 6 show neutral-density surfaces (contours) and zonal density gradients (shaded blocks) of two cross-ridge sections. The contour levels are chosen for approximately uniform vertical spacing in the Brazil Basin, with one additional density surface in the Angola Basin below 4000 m (thin lines). Unshaded zonal density gradients are below the noise level of 5×10^{-8} m^{-1}, estimated from the vertically averaged high-frequency standard deviation of density (3×10^{-3}) and the average station spacing of the 24°S section (70 km). The solid lines following the seafloor topography show the blocking depths for along-flank flows (section 2).

Ignoring eddy-like patterns (e.g., the region below 2500 m at 19°S between stations 156 and 158) the largest zonal density gradients outside the deep western boundary current (DWBC) on the South American continental slope occur in canyons on the western flank of

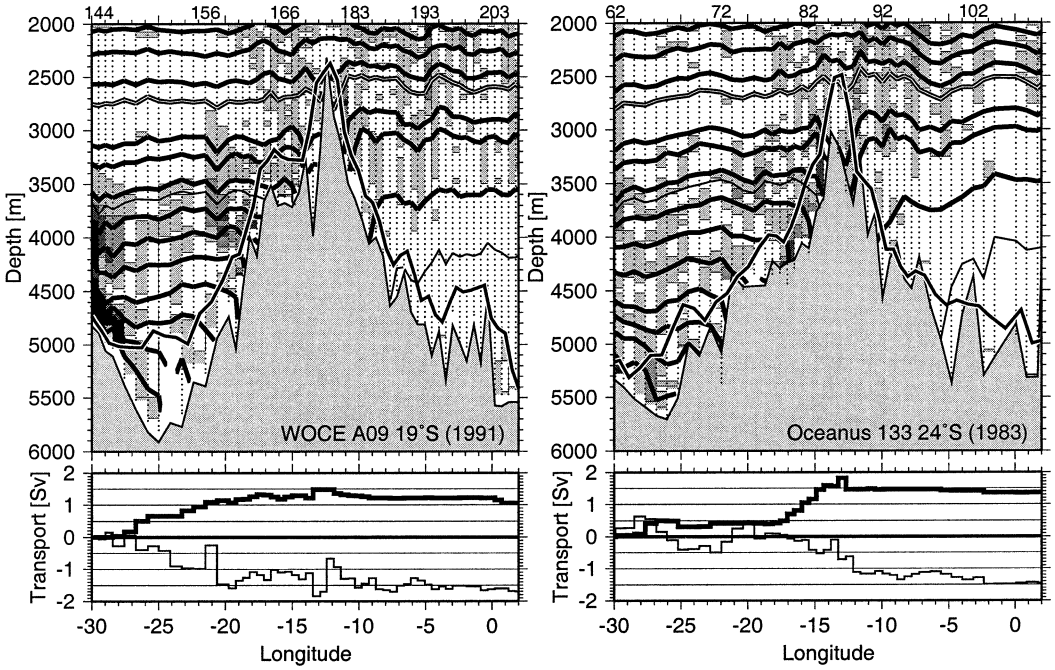

FIG. 6. Zonal sections across the MAR (left) at 19°S and (right) at 24°S. (top) Neutral-density contours (solid lines; 28.05 surface is marked with double lines) and zonal density gradients (values $\geq 5 \times 10^{-8}$ m^{-1} are shaded; contour interval is 10^{-7} m^{-1}); station numbers are indicated above the panels; bathymetric data are taken from water-depth observations at the CTD stations; the mean western-flank slope is $\approx 2 \times 10^{-3}$; topography-following lines indicate blocking depths for along-flank flows (section 2). (bottom) West-to-east accumulated apparent geostrophic transports in the canyons (heavy lines), and geostrophic transports (relative to levels of no motion 1000 m above the blocking depths) in the 500 m immediately above the canyons (thin lines).

the MAR. In the Angola Basin the largest gradients are observed above 3000 m at some distance from the seafloor topography. Over parts of both flanks the isopycnals steepen considerably near the blocking level, consistent with the hydrography in the canyon analyzed by St. Laurent et al. (2001). Elsewhere, primarily in the Angola Basin, the dipping extends well above the crests of the lateral canyon walls. Although the vertical excursions of the isopycnal surfaces on the eastern flank are at least as pronounced as those on the western flank, the corresponding horizontal density gradients (shaded blocks) below 3500 m are significantly smaller because of the weak stratification in the Angola Basin (section 5). Away from the immediate vicinity of the ridge-flank topography, where the densities generally decrease toward the crest, there are regions of reversed gradients in both abyssal basins. The hydrographic patterns in other available cross-ridge sections (Fig. 2) are similar, including the regions of weak zonal density gradients (unshaded) in the Angola Basin at depth and in the western Brazil Basin above $\approx$3500 m.

Topographic blocking prevents the cross-flank pressure gradients in the canyons on the MAR from being balanced geostrophically by along-flank flows (section 2). Ignoring topographic blocking in geostrophic velocities derived from cross-ridge sections therefore leads to unrealistic apparent along-flank transports, as illustrated by the heavy lines in the lower panels of Fig. 6. For this calculation the geostrophic velocities are referenced to the blocking depths and constant-velocity bottom triangles are used. At 19°S the apparent along-flank transports are 1.5 Sv on the western flank and -0.4 Sv on the eastern flank; the corresponding values at 24°S are 1.8 and -0.5 Sv. At both latitudes the blocked apparent transports on the western flank are larger than the corresponding eastern-flank transports, leaving imbalances of >1 Sv. The strongest blocking effect occurs in the 24°S section between 14° and 17°W, where consecutive CTD stations were occupied in what is most likely a continuous valley segment (section 2). At both latitudes (e.g., in the 24°S section at 13°W) there are large apparent transports directly on the ridge crest. These are caused by the geostrophic interpretation of the density gradients between the ridge flanks and the rift valley, which Saunders and Francis (1985) attribute to blocking effects.

When the estimated meridional extent of topographic blocking by the canyon walls is halved—that is, when it is assumed that along-flank flows follow the isobaths into canyons as narrow as 50 km, the blocking depths (which serve as levels of no motion) increase and the apparent transports are correspondingly reduced. In the case of the two sections shown in Fig. 6 the reduction is approximately 30%; that is, the mass-flux imbalances

TABLE 2. Apparent along-flank transports blocked by topography in the zonal sections shown in Fig. 2; imbalances are calculated before rounding.

Lat (°S)	Year	Cruise	Western-flank transport (Sv)	Eastern-flank transport (Sv)	Imbalance (Sv)
5	1993	WOCE A07	2.8	−0.5	2.3
11	1983	Oceanus 133	1.1	−0.6	0.6
11	1994	WOCE A08	0.8	−1.3	−0.5
15	1987	SAVE 2	0.7	−0.8	−0.1
19	1991	WOCE A09	1.5	−0.4	1.1
24	1983	Oceanus 133	1.8	−0.5	1.4
30	1993	WOCE A10	0.3	0.0	0.2

remain of order 1 Sv. Conversely, the apparent transports are increased when higher levels-of-no-motion are chosen. The apparent transports are also increased, by ~30% in this case, when constant-shear bottom triangles are used. In Table 2 the blocked apparent transports of all cross-ridge sections shown in Fig. 2 are listed. North of 19°S there are seamounts decreasing the apparent blocking depths between some station pairs, especially on the eastern flank (section 4). The transports between these stations are not included in the calculations. As expected, the apparent western-flank transports are equatorward while they are poleward on the eastern flank. At most latitudes the cumulated apparent flank transports leave imbalances of order 1 Sv, dominated usually by blocking in the Brazil Basin. The large apparent transports at 5°S are primarily due to the small value of the Coriolis parameter at this latitude. The small apparent transports at 30°S, on the other hand, are primarily related to comparatively shallow ridge-flank canyons south of 25°S.

Immediately above the blocking topography in the Brazil Basin near 20°S float and tracer observations (Hogg and Owens 1999; Ledwell et al. 2000a), as well as an inverse model (St. Laurent et al. 2001) indicate southward velocities of $\approx 2 \times 10^{-3}$ m s^{-1} along the ridge flank. The thin lines in the lower panels of Fig. 6 show the west-to-east cumulated geostrophic transports in the 500 m immediately above the blocking depths relative to reference levels 1000 m above the canyon walls. (These choices are motivated by observations shown in section 4.) At both latitudes there are net western-flank southward transports of 1–1.5 Sv, corresponding to mean velocities of ≈ 1–2×10^{-3} m s^{-1}, that is, consistent with the observations.

4. Meridional sections of cross-flank density gradients

Along the entire latitude range of the tropical and subtropical South Atlantic there are similarities in the topographic organization on the ridge flanks (section 2) and in the main patterns observed in zonal density sections across the MAR (section 3). Because the interannual and the high-frequency hydrographic variabilities are comparable (Fig. 5) meridional sections of isobaric cross-flank density differences can be constructed by combining hydrographic data from 25°, 19°, 9°W and from 2°E (Fig. 2). The distributions of the zonal density gradients at a given latitude (e.g., Fig. 6) imply that the density differences below 2000 m between 25° and 19°W are dominated by the gradients close to the ridge-flank topography, especially by those in the canyons. Both the greater distance between the meridional sections at 9°W and 2°E on the eastern flank and the comparatively smaller zonal density gradients there imply that interpretation of the cross-flank density differences in the Angola Basin is more problematic.

In order to test the assertion that the zonal density differences between meridional sections approximate the corresponding synoptic differences (in zonal sections), repeat-station data from section crossovers are used (Fig. 7). On the western ridge flank (left panel) at 19° and 24°S the density differences between 25° and 19°W (600-km zonal distance) are shown, while the 22°S profiles are calculated from stations at 19° and 15°W (400-km zonal distance; the large open squares in Fig. 3 indicate the positions of the synoptic HRP stations). The western-flank profiles confirm that the synoptic and nonsynoptic zonal density differences in the Brazil Basin are qualitatively and quantitatively similar. The main signal is caused by the dipping of the isopycnal surfaces, which appears as downward-increasing density differences at the bottom of the profiles. Except for the HRP section near 22°S most of the hydrographic stations were occupied somewhat off the deepest axes of the ridge-flank canyons (e.g., Figs. 3 and 4), implying that the maximum density differences along the canyons were rarely sampled. Above the dipping isopycnals on the western flank there is a ~500-m-thick layer where the densities increase toward the crest, consistent with southward along-flank flow near 20°S (section 3). Higher up in the water column the cross-flank density differences below 2000 m do not rise significantly above the temporal variability ($\approx 5 \times 10^{-3}$; Fig. 5).

In comparison with the corresponding values on the western flank, most of the near-bottom density differences on the eastern flank of the MAR between 2°E and 9°W (1100-km zonal distance) are small (Fig. 7). Furthermore, there are systematic offsets of the same order as the near-bottom signals between the synoptic and nonsynoptic density-difference profiles in the Angola Basin at 24° and 30°S. Inspection of the individual station data reveals that the near-constant offset between the two profiles at 24°S is primarily caused by temporal variability at 9°W. The baroclinic differences between the 30°S profiles, on the other hand, are related to temporal changes above 3000 m both at 9°W and at 2°E. Nevertheless, the downward-increasing density differences at the bottom of all eastern-flank profiles shown in Fig. 7 are consistent with isopycnal dipping. The

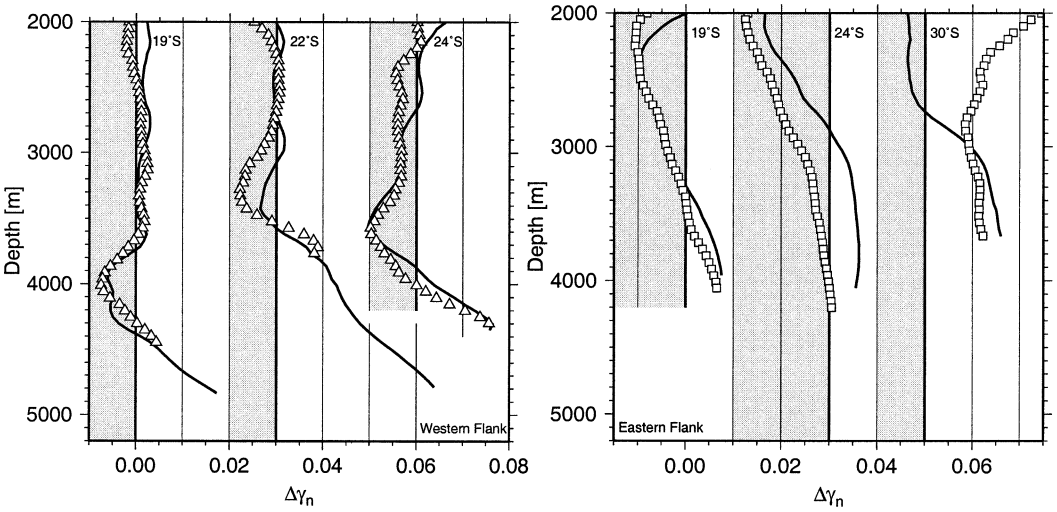

FIG. 7. Cross-flank isobaric neutral-density differences (left) in the Brazil Basin and (right) in the Angola Basin. Solid lines show profiles calculated from synoptic cross-ridge sections (WOCE A09 at 19°S, HRP data at 22°S, Oceanus 133 at 24°S, and WOCE A10 at 30°S); symbols show the corresponding differences between meridional crossover sections (SAVE 6 and A15 on the western flank at 19° and 24°S, 15°W section of A09 and A15 on the western flank at 22°S, and Ajax 1 and A14 on the eastern flank); successive profiles are horizontally offset; profile origins at 0.00, 0.03, (left) 0.06 and (right) 0.05 are marked with heavy grid lines; shaded areas indicate crestward-increasing densities.

observations confirm that the isobaric zonal density differences between nonsynoptic meridional sections approximate the synoptic cross-flank density differences on both flanks.

Figure 8 shows meridional sections of cross-flank density differences along the MAR between 25° and 19°W (left panels) and between 2°E and 9°W (right panels). In the upper panels the differences associated

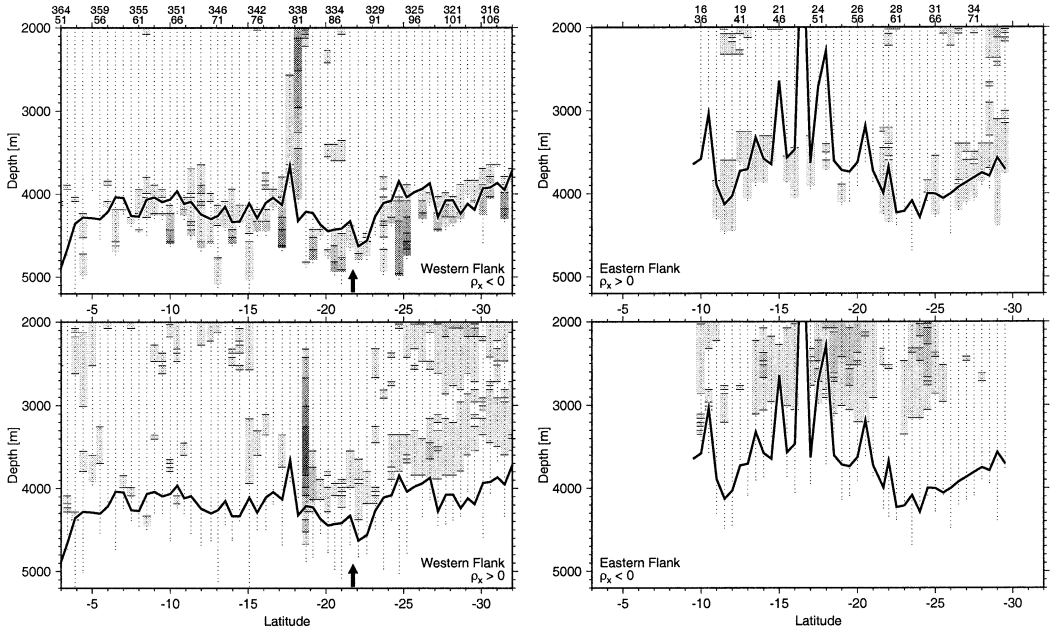

FIG. 8. Isobaric neutral-density differences (left) on the western flank (between 25° and 19°W) and (right) on the eastern flank (between 2°E and 9°W) of the MAR. Densities (top) decreasing and (bottom) increasing toward the ridge crest; i.e., the signatures of isopycnal dipping on the ridge flanks appear in the upper panels; shading indicates density differences $\geq 5 \times 10^{-3}$; contour interval is 10^{-2}; station numbers of the deep-basin sections are indicated above the ridge-flank station numbers above the upper panels. The solid lines show the topographic blocking depths at (left) 19°W and (right) 9°W; the arrows on the western flank near 21°45′S mark the canyon analyzed by St. Laurent et al. (2001).

with crestward-decreasing densities (dipping isopycnals; positive values in Fig. 7) are plotted and the lower panels show the density differences of opposite sign. Only values above the temporal variability are shaded. In order to compensate for the nonzonality of the ridge-flank canyons in the Angola Basin (Figs. 1 and 2) the meridional portion of the 2°E section between 8° and 28°S is shifted 2° to the south before calculating the zonal density differences. The solid lines show the topographic blocking depths for along-flank flows (section 2) at 19° and 9°W. The large positive and negative cross-flank density differences in the Brazil Basin near 19°S extending more than 2000 m above the ridge-flank topography are caused by anomalous hydrographic conditions encountered during the WOCE A15 cruise at 19°W (Fig. 5; see also Weatherly et al. 2002).

On the western flank of the MAR the density differences associated with isopycnal dipping (Fig. 8 top left) are observed along the entire latitude range of the Brazil Basin. Consistent with cross-ridge hydrographic sections (e.g., Fig. 6), the crestward density drops on the western flank are largely confined to the canyons. The layer of crestward-increasing densities above the canyons is only observed south of ≈15°S (Fig. 8 bottom left). The lower limit of this layer approximately follows the seafloor topography. The deep cross-flank density differences in the Angola Basin (Fig. 8 right) are generally smaller and the patterns are more ambiguous as discussed above. Nevertheless, signatures consistent with dipping isopycnals (upper-right panel) are observed along the entire latitude range of the Angola Basin where data are available. Near 9°W there are a number of islands and seamounts causing the peaks in the apparent blocking depths. Where there are no seamounts (e.g., south of 25°S), the dipping of the isopycnal surfaces on the eastern ridge flank commonly extends several hundred meters above the blocking topography. Crestward-increasing densities occur on the eastern flank as well (lower-right panel). They are observed higher up in the water column (2000–3000 m) than those on the western flank but even here there are indications for their lower extent following the seafloor topography to some degree.

5. Vertical mixing of density, temperature, and salinity

The observations presented in section 4 reveal vertical dipoles in the cross-flank density gradients on both sides of the MAR in the South Atlantic. This pattern is qualitatively similar to the one observed in (nonrotating) laboratory experiments of bottom-intensified mixing of stratified fluid on planar slopes (Phillips et al. 1986). Therefore, it is reasonable to investigate the extent to which the cross-flank density gradients can be accounted for by diapycnal mixing. Without horizontal mixing and without source/sink terms the density equation can be written (e.g., Polzin et al. 1997)

$$w_* = w + (\rho_z)^{-1}(\rho_t + \mathbf{u}\cdot\nabla\rho) = (\rho_z)^{-1}(\kappa\rho_z)_z, \quad (2)$$

where $\mathbf{u}$ and w denote horizontal and vertical velocities, respectively. While also having units of velocity w_*, which is defined by expression (2), is not necessarily associated with any motion (apart from parameterized eddies) but is directly related to the buoyancy flux. In a steady state $w_* < 0$ implies densification following the flow. (We stress that even in this case the velocity field can be purely horizontal without any vortex stretching taking place.) The analysis of HRP data from the western flank of the MAR by St. Laurent et al. (2001) implies a vertical w_* dipole with positive values in the canyons and negative ones above, similar to the bottom-intensified mixing run of the 2D model of Thompson and Johnson (1996). In both cases the buoyancy required to reduce the densities near the bottom is removed from overlying water. This is a direct consequence of bottom-intensified mixing in regions where the density stratifications do not decrease too strongly with increasing depth—that is, where $(\kappa\rho_z)_z > 0$, as is the case in the deep Brazil Basin (Polzin et al. 1997).

In order to determine to what extent the magnitudes of the observed cross-flank density gradients are consistent with vertical mixing expression (2) is applied to hydrographic profiles from the abyssal basins on both sides of the MAR. For simplicity we solve the time-varying problem in a horizontally nondivergent flow-following framework, making it formally equivalent to a model in one spatial dimension because the terms involving velocities in expression (2) vanish. This simplification assumes that the timescale over which mixing can act does not vary significantly across the layer where mixing is intense (Thompson and Johnson 1996). The density equation is solved numerically with insulating and radiating boundary conditions at the seabed and at 1000 m, respectively. Initial hydrographic profiles are constructed by averaging data from the meridional sections at 25°W (Brazil Basin) and at 2°E (Angola Basin); the left panel of Fig. 9 shows the resulting buoyancy frequencies. Because of the large height of the MAR, expression (2) is applied to profiles cut off at 5500 m (lower flanks), at 4500 m (midflanks), and at 3500 m (upper flanks). Motivated by HRP observations (Polzin et al. 1997; St. Laurent et al. 2001) exponentially upward-decreasing diffusivity profiles with 500-m decay scales are constructed; a background value of 10^{-5} m^2 s^{-1} is added at all depths. The bottom diffusivity on the lower-flank in the Brazil Basin is set to 4×10^{-3} m^2 s^{-1}, the ensemble-averaged value in the advection–diffusion canyon model of St. Laurent et al. (2001) (L. C. St. Laurent 2002, personal communication). The exponential diffusivity profiles are scaled with the ratios of the mean vertical density gradient in the bottom 1500 m of the lower-flank Brazil Basin profile to the corresponding values in the profiles used for the particular runs. This amounts to the assumption that the dissipation profiles (as opposed to the diffusivity profiles) are the

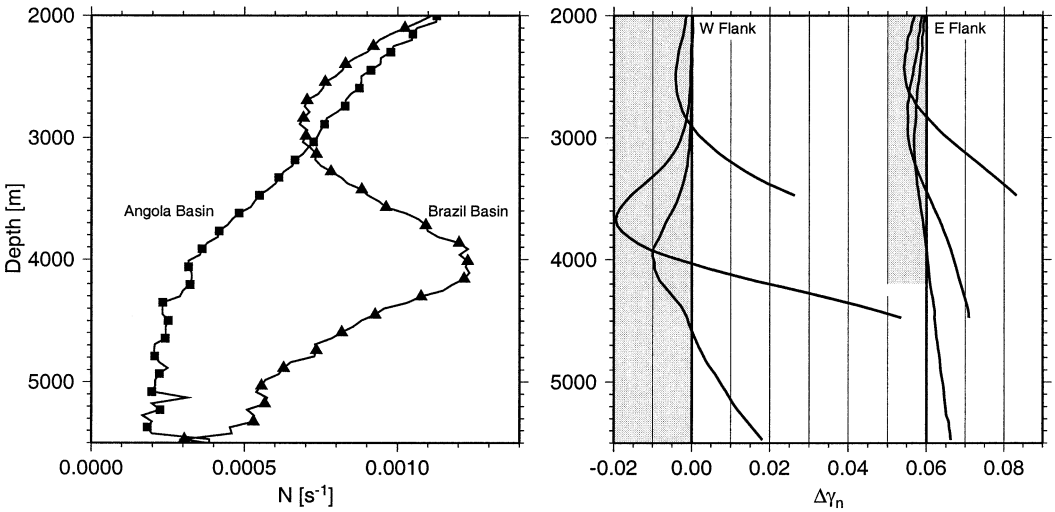

FIG. 9. (left) Mean buoyancy-frequency profiles of the Brazil Basin (along 25°W) and of the Angola Basin (along 2°E). (right) Isobaric neutral-density differences (initial minus final values) after 4.5 yr of bottom-intensified vertical mixing applied to hydrographic profiles from the abyssal basins; separate profiles are shown for the lower (5500 m), middle (4500 m), and upper flanks (3500 m); eastern-flank profiles are horizontally offset by 0.05; shaded areas indicate densification caused by mixing ($w_* < 0$).

same across both ridge flanks. This scaling primarily affects the solutions in the deep Angola Basin where the stratification is so weak that the effects of mixing are insignificant without it. The running time of the model is somewhat arbitrary; based on results derived by St. Laurent et al. (2001), we chose 4.5 yr, the expected time a water parcel spends in a 500-m-deep canyon on a 10^{-3} slope while moving horizontally with a velocity of 3.5×10^{-3} m s^{-1}.

Figure 9 right shows the temporal effects of vertical mixing applied to the density profiles from the abyssal basins. As expected the simulated mixing results in vertical w_* dipoles with layers of mean densification overlying bottom layers where the time-averaged buoyancy fluxes are positive. Unexpectedly, the modeled temporal density differences are qualitatively and quantitatively similar to observed cross-flank density gradients, especially to those on the western flank near 20°S (Fig. 7). Even though the diffusivities of the individual model runs are scaled with the inverse of the vertical density gradients, the modeled density differences are particularly large where the stratification is strongest. Consistent with the lower-left panel of Fig. 8 the largest density differences associated with negative w_* on the western ridge flank occur between 3500 and 4000 m. On the eastern flank the agreement between the temporal model results and the observed cross-flank density differences is less close. Nevertheless there are similarities, for example in the cross-flank distribution of the density gradients. On the upper flanks, where the stratifications on both sides of the crest are similar, there are no significant cross-ridge differences in the magnitudes of either the modeled or the observed density gradients. Farther down the ridge flanks, on the other hand, the cross-flank density gradients in the Angola Basin are significantly smaller than the corresponding gradients in the Brazil Basin, both in the model (Fig. 9) and in observations (Fig. 6).

Given the strong effect of vertical mixing on the ridge-flank density field it is reasonable to investigate to what extent the cross-flank gradients of temperature and salinity can be accounted for by the same process. Figure 10 left shows *T*–*S* diagrams from the 24°S section between 25°W and 2°E. The crest of the MAR penetrates approximately to the 28.05 neutral surface (Fig. 6). At crest level there are zonal isopycnal differences of order 0.05 psu and 0.23°C on the western ridge flank east of 19°W, while the gradients further west and on the eastern flank are much smaller. Below crest depth the water in the Brazil Basin shows a slight up-flank cooling/freshening on isopycnal surfaces. Similar crestward cooling/freshening is observed on the western flank in all cross-ridge sections shown in Fig. 2.

Along the flow path isopycnal cooling/freshening is expected from the *T*–*S* curvature associated with the salinity maximum of North Atlantic Deep Water (NADW) in the Brazil Basin, because vertical mixing tends to linearize the *T*–*S* properties. In order to determine the quantitative effects of mixing, heat and salt analogues of expression (2) are solved numerically. Diffusivity profiles and the running time of 4.5 yr are chosen as before. Because of comparatively large meridional *T*–*S* gradients in the deep South Atlantic (e.g., Siedler et al. 1996) initial profiles are constructed from 50-dbar-averaged hydrographic profiles at 24°S, 19°W (Brazil Basin) and at 24°S, 2°E (Angola Basin) rather than by meridionally averaging hydrographic data as before. The midflank solutions are shown in the right

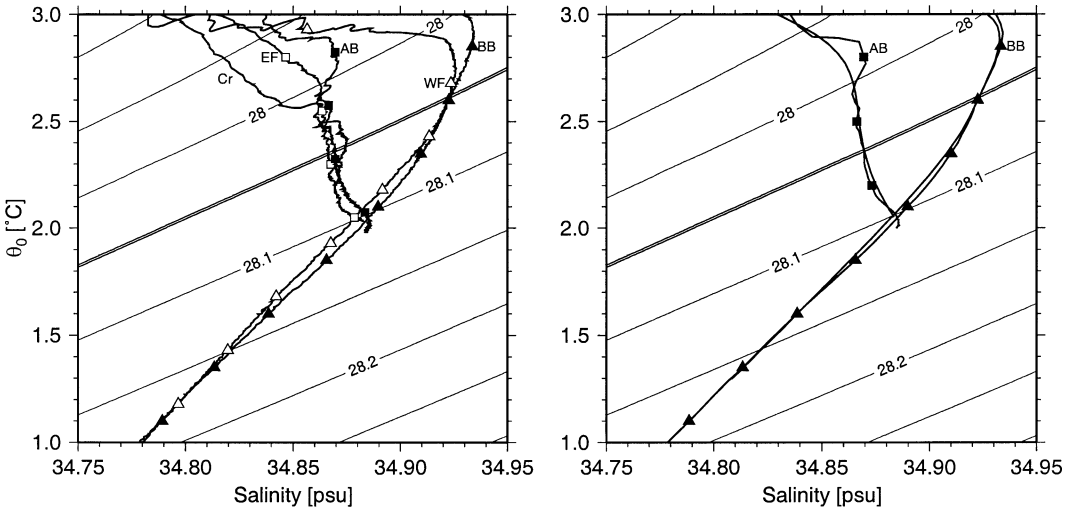

FIG. 10. The *T–S* properties at 24°S. Neutral-density contour interval is 0.05; 28.05 contours near the crest depth of the MAR are marked with double lines (cf. Fig. 6). (left) Observed properties in the Brazil Basin (BB; 25°W), on the western flank (WF; 19°W), over the ridge crest (Cr; 13°W), on the eastern flank (EF; 9°W), and in the Angola Basin (AB; 2°E). (right) Vertical-mixing effects on 50-dbar-averaged *T–S* properties from the abyssal basins; initial profiles are marked as in the left panel; postrun profiles are plotted as solid lines without symbols.

panel of Fig. 10. Comparison between the observed *T–S* properties on the ridge flanks and the model results indicates that the zonal temperature and salinity gradients at 24°S between 19°W and the ridge crest cannot be accounted for by vertical mixing. They are more likely set by the combined effects of horizontal advection and mixing, neither of which is included in our simple model. The *T–S* signatures of vertical mixing are subtle in comparison. While we cannot separate the effects of horizontal and vertical mixing in the observations, it is nevertheless noted that the bottom-most parts of the profiles are generally consistent with vertical mixing. The eastern-flank *T–S* properties of the densest water ($\gamma_n \approx 28.1$) at 24°S (Fig. 10 left), for example, tend toward those in the deep Angola Basin where the ''hook'' at the bottom of the profile indicates the presence of remnant Antarctic Bottom Water (AABW). After the model is applied to the Angola Basin profile, the AABW signature disappears (Fig. 10 right), implying that this difference between the ridge-flank and the basin-interior profiles is consistent with vertical mixing acting on a timescale of several years. Crestward isopycnal cooling/freshening of the bottom water on the eastern ridge flank, consistent with upflank flow and mixing in canyons, is observed in all available cross-ridge sections shown in Fig. 2.

6. Discussion

a. Cross-flank density gradients and along-flank flows

Diapycnal mixing redistributes buoyancy in the water column. Assuming that there is no significant density flux across the seabed (e.g., Thurnherr et al. 2002), the overlying water must act as the source for the buoyancy required to reduce the density of the deepest water. Observations indicate that the magnitudes of the buoyancy fluxes above the western flank of the MAR in the South Atlantic decrease upward with a decay scale of several hundred meters (Polzin et al. 1997; St. Laurent et al. 2001). This implies densification of water at and below crest level as a consequence of mixing. Our observation of a layer of crestward-increasing densities on the western flank of the MAR south of 15°S appears to be the first oceanographic evidence for densification that is most likely caused by bottom-intensified vertical mixing. This conclusion is largely based on the similarities between numerical solutions of the density equation and observed cross-flank density gradients, which are qualitatively consistent with laboratory experiments of bottom-intensified mixing on planar slopes (Phillips et al. 1986). [Thompson and Johnson (1996) also note that the temporal density gradients caused by diapycnal diffusion acting on basin-interior profiles are similar to observed cross-flank gradients.] Since the along-flank horizontal density variations in our study region are small (e.g., DeMadron and Weatherly 1994) the simplest zonal velocity field that is consistent with the observations is uniform crestward flow in the layer of strong mixing. This is irreconcilable with the meridionally integrated stream function on the ridge flank of St. Laurent et al. (2001). Uniform horizontal flow is not the only possible solution, however. Based on our data we cannot infer the details of the advective terms of expression (2), but we note that neither the horizontal nor the vertical components can necessarily be neglected. When representative values for $|u| \approx 5 \times 10^{-3}$ m s^{-1} (St. Laurent et al. 2001), $|\rho_x| \approx 10^{-7}$ m^{-1} (Fig. 6), and $N \approx 7.5 \times 10^{-4}$ s^{-1} (Fig. 4) are chosen, the magnitudes

of the cross-flank and the vertical advection terms in Eq. (2) are equal for vertical velocities of order 10^{-5} m s^{-1}. Virtually nothing is known about the vertical-velocity field on the ridge flanks but values of order 10^{-5} m s^{-1} are consistent with up-flank flow in sloping canyons ($|w| = |u| \tan\alpha$), and with vertical velocities inferred in other regions of rough topography (Thurnherr et al. 2002). Last, we note that the laboratory experiments of Phillips et al. (1986) show that bottom-intensified mixing can cause cross-slope density-gradient dipoles even in the presence of horizontal and vertical advection.

In contrast to the cross-flank density gradients, the main horizontal patterns in the temperature and salinity fields on the flanks of the MAR in the South Atlantic cannot be accounted for without taking horizontal advection and mixing into account. Vertical mixing has an indirect effect on the horizontal property distributions because of advection by the horizontal circulations associated with the mixing. Numerical models suggest that the mixing-driven flows along midocean ridges may be associated with transports similar to DWBCs and that the expected net transports on smooth slopes are equatorward on western flanks and poleward on eastern flanks of meridional ridges (Thompson and Johnson 1996; Huang and Jin 2002). The topographic blocking depth in the Brazil Basin south of 15°S approximately coincides with the level where the buoyancy fluxes associated with the bottom-intensified mixing change sign, implying that the lower, equatorward portion of the along-flank flow is blocked. This provides a plausible explanation for the poleward flank flow near 20°S inferred from float data (Hogg and Owens 1999), from tracer dispersal (Ledwell et al. 2000), from an inverse model (St. Laurent et al. 2001), and from simple geostrophic calculations (section 3). (It will be noted that no β effect is required for this poleward flow along the eastern boundary of the Brazil Basin.) The extent to which the topography blocks poleward flow along the eastern flank of the MAR is less clear but it is noted that tracer distributions at 11° and 24°S are consistent with an equatorward DWBC along the ridge in the Angola Basin (Warren and Speer 1991).

The cross-flank density gradients on both sides of the MAR in the South Atlantic extend below the blocking topography into the ridge-flank canyons. Neglecting blocking effects in numerical models and geostrophic estimates of the circulation (including inverse models) leads to unrealistic along-flank transports of significant magnitudes (up to 3 Sv in our geostrophic calculations) and corresponding underestimates of the diapycnal fluxes in ridge-flank canyons. While the apparent along-flank flows are of opposite signs on the two ridge flanks, they usually do not balance each other, leaving deficits up to 2 Sv—that is, of the same order as typical a priori uncertainties associated with cross-oceanic volume transports used in box-inverse calculations (e.g., Wunsch 1996). [The corresponding errors in the diapycnal fluxes are more difficult to assess, especially because the models are often set up to treat these as ''residuals'' (e.g., Vanicek and Siedler 2002).] The problem is even more severe for inversions that span the equator because the blocked apparent flank flows form convergences and divergences there. On comparatively smoother ridges, such as the East Pacific Rise, topographic blocking effects are expected to be weaker.

b. Topographic organization and diapycnal mixing

The global distribution of seafloor roughness (Gille et al. 2000) implies that the topographic variance of the MAR in the tropical and subtropical South Atlantic is not unique. In our study region the roughness of the ridge is organized into a large number of cross-flank canyons. A comparison with Fig. 6 suggests that much of the enhanced mixing observed on the western flank of the MAR in the South Atlantic (Polzin et al. 1997) is most likely confined below the topographic blocking depth. Therefore, it seems reasonable to consider the possibility that some of the enhanced mixing is related to the presence of canyons. Parameterizations of dissipation based on topographic variance (e.g., Jayne and St. Laurent 2001), on the other hand, assume that the topographic organization is not important for the processes responsible for the observed high levels of mixing. This is arguably valid if the enhanced dissipation is primarily driven by tidal flows (Polzin et al. 1997; Ledwell et al. 2000b).

However, mechanisms other than tidally forced internal-wave breaking operate in the canyons on the MAR flanks. Perhaps the strongest argument for the tides being the dominant energy source for the enhanced mixing on rough topography is the apparent weakness (compared to the tides) of low-frequency and mean flows in the eastern Brazil Basin (Polzin et al. 1997). It is not clear if this argument holds in the ridge-flank canyons, where diapycnal mixing causes along-axis pressure gradients and down-gradient mean flows (St. Laurent et al. 2001). Observations from the rift valley near 36°N, which is characterized by a similar along-axis density gradient ($\approx 10^{-7}$ m^{-1}) and comparable topographic scales (depth $\approx$1000 m, width $\approx$20 km), show along-axis velocities exceeding 0.2 m s^{-1}, strong vertical shear, as well as topographic lee waves in the vicinity of a sill partially blocking the persistent along-valley current (Thurnherr and Richards 2001; Thurnherr et al. 2002). The flow across the sill is similar to those observed in a number of deep oceanic fracture zones and passages (e.g., Garner 1972; Hogg et al. 1982; Polzin et al. 1996; Hall et al. 1997). Cross-sill flows are easily missed in large-scale surveys, such as the ones analyzed by Polzin et al. (1997) and by St. Laurent et al. (2001), because of their small horizontal extents (Thurnherr et al. 2002). In the data of Smith and Sandwell (1997) topographic excursions of several hundred meters along the axes of ridge-flank canyons are com-

mon. Recently acquired Seabeam data from the western flank of the MAR near 20°S (Ledwell et al. 2000a) indicate that many of the topographic highs along the canyon axes extend across their entire widths and that their vertical extents can be significantly underestimated in the Smith and Sandwell (1997) seafloor topography. Therefore, it is not yet clear whether tidally generated breaking internal waves or canyon-related processes, such as hydraulic cross-sill flows, dominate the mixing on the flanks of the MAR in the South Atlantic and elsewhere. As a consequence, topographic variance may not provide an accurate parameterization for mixing over all parts of the global midocean ridge system.

Acknowledgments. We thank John Toole for providing the HRP data used in this study. Nelson Hogg pointed out the consistency of his float data with our inference of southward along-flank flow in the Brazil Basin, which considerably strengthens our argument. Lou St. Laurent and two reviewers constructively criticized the manuscript. The analysis was carried out in the context of the WOCE AIMS Deep Basin Experiment Synthesis project (NSF Grant OCE-9911148).

APPENDIX

Valley-Detection Algorithm

In order to determine a quantitative measure for the organization of the roughness on the flanks of the MAR in the South Atlantic, we devised a simple valley-detection algorithm:

1) Find local extrema $\geq$250 m in meridional sections zonally separated by 5′ (Fig. 1).
2) For each maximum,
   a) generate list of neighbors, according to the following rules:
      i) zonal distance $\leq$18 km,
      ii) meridional distance $\leq$15 km, and
      iii) mean slope $\leq 10^{-1}$, and then
   b) connect to nearest neighbor.
3) Delete valleys segments shorter than 40 km.
4) Repeat steps 1–3 with zonal sections to find quasi-meridional valleys.

The parameter values are chosen so that the final result conservatively approximates a visual assessment of the same region (e.g., Fig. 3).

A comparison with output from another valley-detection algorithm (Chang et al. 1998) indicates that both detect all major valleys, including ridge-flank canyons and rift-valley segments. The algorithm of Chang et al. (1998) requires only one parameter, called ''profile length,'' which determines how many neighboring points are considered during the search for valley-floor candidates. For the region shown in Fig. 3, a ''profile length'' of 30 full-resolution Smith and Sandwell (1997) pixels yields a similar (within 5%) total length of the zonal valley segments when compared with the output of our algorithm without the 40-km-length restriction, while 25% more meridional valleys are detected. This difference is primarily the result of our minimum-depth restriction; that is, a significant portion of the meridional valley segments detected by the algorithm of Chang et al. (1998) are less than 250 m deep.

REFERENCES

Baines, P. G., 1987: Upstream blocking and airflow over mountains. *Annu. Rev. Fluid Mech,* **19,** 75–97.

Chang, Y.-C., G.-S. Song, and S.-K. Hsu, 1998: Automatic extraction of ridge and valley axes using the profile recognition and polygon-breaking algorithm. *Comput. Geosci.,* **24,** 83–93.

DeMadron, X. D., and G. Weatherly, 1994: Circulation, transport and bottom boundary layers of the deep currents in the Brazil Basin. *J. Mar. Res.,* **52,** 583–638.

Garner, D. M., 1972: Flow through the Charlie-Gibbs fracture zone, Mid-Atlantic Ridge. *Can. J. Earth Sci.,* **9,** 116–121.

Garrett, C., P. MacCready, and P. Rhines, 1993: Boundary mixing and arrested Ekman layers: Rotating stratified flow near a sloping boundary. *Annu. Rev. Fluid Mech.,* **25,** 291–323.

Gille, S. T., M. M. Yale, and D. T. Sandwell, 2000: Global correlation of mesoscale ocean variability with seafloor roughness from satellite altimetry. *Geophys. Res. Lett.,* **27,** 1251–1254.

Gregg, M. C., 1998: Estimation and geography of diapycnal mixing in the stratified ocean. *Physical Processes in Lakes and Oceans,* J. Imberger, Ed., Amer. Geophys. Union, 305–338.

Hall, M. M., M. McCartney, and J. A. Whitehead, 1997: Antarctic Bottom Water flux in the equatorial western Atlantic. *J. Phys. Oceanogr.,* **27,** 1903–1926.

Helfrich, K. R., 1995: Time-dependent two-layer hydraulic exchange flows. *J. Phys. Oceanogr.,* **25,** 359–373.

Hogg, N. G., and W. B. Owens, 1999: Direct measurement of the deep circulation within the Brazil Basin. *Deep-Sea Res.,* **46B,** 335–353.

——, P. Biscaye, W. Gardner, and W. J. Schmitz, 1982: On the transport and modification of Antarctic Bottom Water in the Vema Channel. *J. Mar. Res.,* **40,** 231–263.

Huang, R. X., and X. Jin, 2002: Deep circulation in the South Atlantic induced by bottom-intensified mixing over the midocean ridge. *J. Phys. Oceanogr.,* **32,** 1150–1164.

Jayne, S. R., and L. C. St. Laurent, 2001: Parameterizing tidal dissipation over rough topography. *Geophys. Res. Lett.,* **28,** 811–814.

Johnson, G. C., P. E. Robbins, and G. E. Hufford, 2001: Systematic adjustments of hydrographic sections for internal consistency. *J. Atmos. Oceanic Technol.,* **18,** 1234–1244.

Keller, G. H., S. H. Anderson, and J. W. Lavelle, 1975: Near-bottom currents in the Mid-Atlantic Ridge rift valley. *Can. J. Earth Sci.,* **12,** 703–710.

Klinck, J. M., 1996: Circulation near submarine canyons: A modeling study. *J. Geophys. Res.,* **101,** 1211–1223.

Ledwell, J. R., T. Donoghue, B. Guest, P. Lemmond, C. Sellers, and N. Cortes, 2000a: R/V *Knorr* cruise 161-6. WHOI cruise report, in press. [Available online at http://www.whoi.edu/science/AOPE/cofdl/bbasin/publications/index.html.]

——, E. T. Montgomery, K. L. Polzin, L. C. St. Laurent, R. W. Schmitt, and J. M. Toole, 2000b: Evidence for enhanced mixing over rough topography in the abyssal ocean. *Nature,* **403,** 179–182.

Morris, M. Y., M. M. Hall, L. C. St. Laurent, and N. G. Hogg, 2001: Abyssal mixing in the Brazil Basin. *J. Phys. Oceanogr.,* **31,** 3331–3348.

Munk, W., 1966: Abyssal recipes. *Deep-Sea Res.,* **13,** 707–730.

Phillips, O. M., 1970: On flows induced by diffusion in a stably stratified fluid. *Deep-Sea Res.,* **17,** 435–443.

——, J.-H. Shyu, and H. Salmun, 1986: An experiment on boundary mixing: Mean circulation and transport rates. *J. Fluid. Mech.*, **173,** 473–499.

Pierrehumbert, R. T., and B. Wyman, 1985: Upstream effects of mesoscale mountains. *J. Atmos. Sci.*, **42,** 977–1003.

Polzin, K. L., K. G. Speer, J. M. Toole, and R. W. Schmitt, 1996: Intense mixing of Antarctic Bottom Water in the equatorial Atlantic Ocean. *Nature,* **380,** 54–57.

——, J. M. Toole, J. R. Ledwell, and R. W. Schmitt, 1997: Spatial variability of turbulent mixing in the abyssal ocean. *Science*, **276,** 93–96.

Saunders, P. M., and T. J. Francis, 1985: The search for hydrothermal sources on the Mid-Atlantic Ridge. *Progress in Oceanography*, Vol. 14, Pergamon, 527–536.

Siedler, G., T. J. Müller, R. Onken, M. Arhan, H. Mercier, B. A. King, and P. M. Saunders, 1996: The zonal WOCE sections in the South Atlantic. *The South Atlantic: Present and Past Circulation,* G. Wefer et al., Eds., Springer Verlag, 45–62.

Smith, W. H. F., and D. T. Sandwell, 1997: Global seafloor topography from satellite altimetry and ship depth soundings. *Science*, **277,** 1956–1962.

St. Laurent, L. C., J. M. Toole, and R. W. Schmitt, 2001: Buoyancy forcing by turbulence above rough topography in the abyssal Brazil Basin. *J. Phys. Oceanogr.*, **31,** 3476–3495.

Stommel, H., and A. B. Arons, 1972: On the abyssal circulation of the world ocean. Part 5: Influence of bottom slope on broadening of inertial boundary currents. *Deep-Sea Res.*, **19,** 707–718.

Stramma, L., and R. G. Peterson, 1990: The South-Atlantic Current. *J. Phys. Oceanogr.*, **20,** 846–859.

Thompson, L., and G. C. Johnson, 1996: Abyssal currents generated by diffusion and geothermal heating over rises. *Deep-Sea Res.*, **43,** 193–211.

Thurnherr, A. M., and K. J. Richards, 2001: Hydrography and high-temperature heat flux of the Rainbow hydrothermal site (36°14′N, Mid-Atlantic Ridge). *J. Geophys. Res.*, **106,** 9411–9426.

——, ——, C. R. German, G. F. Lane-Serff, and K. G. Speer, 2002: Flow and mixing in the rift valley of the Mid-Atlantic Ridge. *J. Phys. Oceanogr.*, **32,** 1763–1778.

Vanicek, M., and G. Siedler, 2002: Zonal fluxes in the deep water layers of the western South Atlantic Ocean. *J. Phys. Oceanogr.*, **32,** 2205–2235.

Warren, B. A., and K. G. Speer, 1991: Deep circulation in the eastern South Atlantic Ocean. *Deep-Sea Res.*, **38,** 281–322.

Weatherly, G., M. Arhan, H. Mercier, and W. Smethie Jr., 2002: Evidence of abyssal eddies in the Brazil Basin. *J. Geophys. Res.*, **107,** 3027, doi:10.1029/2000JC000648.

Wunsch, C., 1970: On oceanic boundary mixing. *Deep-Sea Res.*, **17,** 293–301.

——, 1996: *The Ocean Circulation Inverse Problem.* Cambridge University Press, 442 pp.